Journal of
Materials Chemistry C

Materials for optical, magnetic and electronic devices

Accepted Manuscript

This article can be cited before page numbers have been issued, to do this please use: S. SHOME and S. Konar, *J. Mater. Chem. C*, 2026, DOI: 10.1039/D5TC03535J.

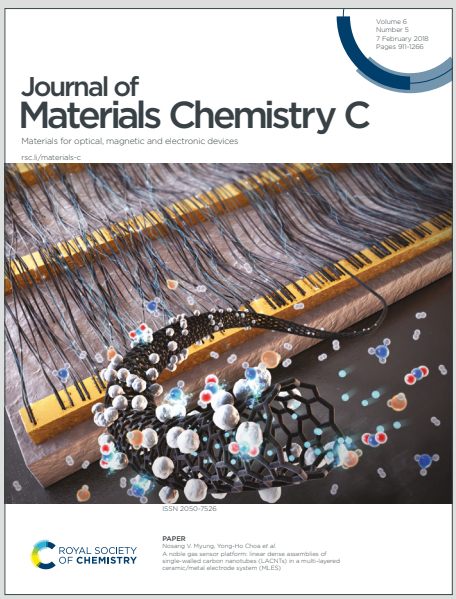

ROYAL SOCIETY OF CHEMISTRY

rsc.li/materials-c

View Article Online
DOI: 10.1039/D5TC03535J

ARTICLE

Hysteresis-Encoded Thermometry in the Cryogenic Regime Using Dy-Single-Molecule Magnet

Shraoshee Shome,[a] and Sanjit Konar*[a]

Received 00th January 20xx,
Accepted 00th January 20xx

DOI: 10.1039/x0xx00000x

Precise cryogenic thermometry (< 10 K) in single-molecule magnets (SMMs) remains a critical challenge, as conventional approaches often suffer from poor sensitivity and limited applicability. To address this, we present a hysteresis-based thermometry approach with a Dy(III)- SMM, which leverages key magnetic parameters from hysteresis loops to provide a sensitive alternative. Three distinct hysteresis parameters: saturation magnetisation (M_S), remanent magnetisation (M_R), and loop area (A) have been used in the 2-8 K regime for thermometry. All three parameters decrease monotonically with increasing temperature, and this temperature dependence results in excellent relative thermal sensitivities (S_r), following the trend $S_r^A > S_r^R > S_r^S$. Further scan rate-dependent analyses were performed, showing negligible variations across different sweep rates, confirming the stability of the thermometric response under varying scan conditions. This work represents the first demonstration of hysteresis-based thermometry in SMMs, providing a versatile route for cryogenic sensing by utilising the intrinsic magnetisation dynamics, with promising implications for quantum and low-temperature device applications.

Introduction

Single-molecule magnets (SMMs) have emerged as promising candidates for next-generation quantum technologies, including quantum information processing, molecular spintronics, and high-density data storage.[1-8] Their unique ability to retain magnetisation at the molecular level, coupled with tunable magnetic relaxation dynamics, makes them attractive building blocks for nanoscale devices.[9-16] However, most of the SMMs operate intrinsically in the cryogenic regime, where spin relaxation is sufficiently slow to sustain the quantum coherence.[17-20] Precise thermometry below 10 K is particularly important in this regard as (i) at these region, small thermal fluctuations can strongly influence magnetic relaxation pathways, quantum tunnelling rates, and spin–phonon interactions, critically affecting the physical behaviour of SMMs; (ii) from a technological perspective, accurate sub-10 K temperature readout is essential for calibration and reliable operation of cryogenic quantum devices and low-temperature magnetic memory systems.[21-23] Traditional approaches to temperature sensing in SMMs have relied mostly on luminescence thermometry (based on emission band shift, lifetime, and intensity, etc.).[24-42] Recently, magneto-thermometry using relaxation time (τ), magnetic susceptibility (χ)[43], magneto-chiral dichroism (MCD)[17], and magnetic circularly polarised luminescence (MCPL)[44], etc., has also been reported. While these methods have been successful at moderate cryogenic as well as high temperatures, their sensitivity and reliability often deteriorate below 10 K. For example, below 10 K, luminescence thermometry faces challenges due to reduced Boltzmann redistribution[45], magneto-thermometry using 1/χ fails below 10 K due to deviation from Curie behaviour (< 10 K magnetic anisotropy dominates), and magneto-thermometry using τ fails due to the dominance of temperature-independent relaxation, such as quantum tunnelling of magnetisation (QTM)[43]. The MCD-based thermometry has a strong dependence on transmission geometry and magnetic field stability, making real-life implementation technically challenging, and it is further restricted to SMMs that exhibit MCD, thereby narrowing its applicability.[17] Thus, there is a pressing need for innovative thermometry strategies specifically tailored to the deep-cryogenic (sub-10 K) regime, which can provide an intrinsic, reliable, and sensitive readout of temperature without the limitations of existing methods.

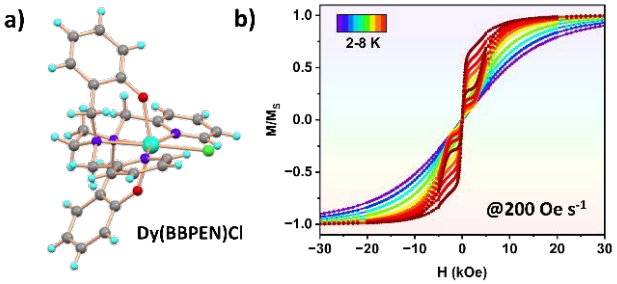

Figure 1: a) The molecular structure of complex 1, b) variable temperature hysteresis in 2-8 K temperature range (200 Oe s^{-1}). (Colour code: Dy-cyan, C-grey, N-blue, O-red, Cl-green, H-light blue)

Herein, we introduce a hysteresis-based thermometry strategy that exploits the intrinsic temperature dependence of magnetic hysteresis loop characteristics as thermal markers. For this purpose,

[a] Department of Chemistry, Indian Institute of Science Education and Research Bhopal, Bhopal Bypass Road, Bhauri, Madhya Pradesh, India- 462066.

† Supplementary Information available: Experimental details, PXRD patterns, FT-IR spectra, TGA data, and additional measurement information. See DOI: 10.1039/x0xx00000x

View Article Online
DOI: 10.1039/D5TC03535J

ARTICLE

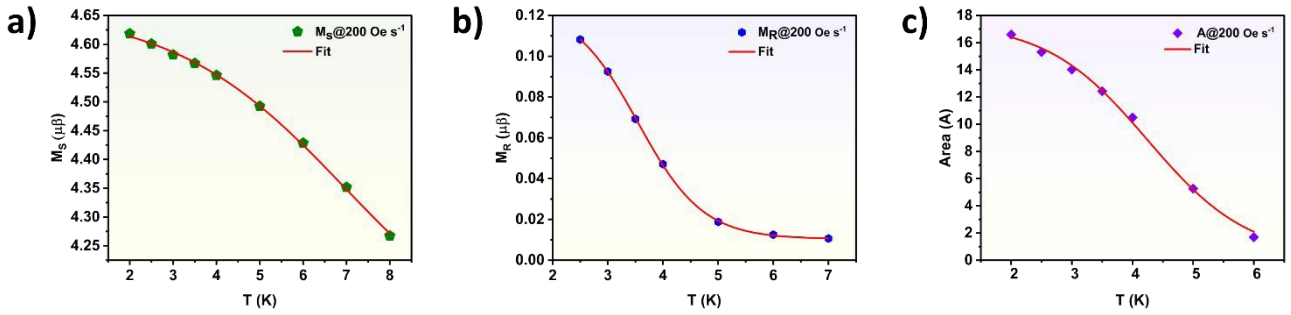

Figure 2: The temperature dependence of the thermometry parameters a) saturation magnetisation, b) remanent magnetisation, and c) area fitted to equation 1 in Origin Pro.

we employed the air-stable Dy(BBPEN)Cl[46] SMM (H_2BBPEN = N,N′-bis(2-hydroxybenzxyl)-N,N′-(2-pyridylmethyl)ethylenediamine, complex 1, Figure 1). Complex 1 shows U_{eff} of 708 K and is particularly suited for such studies owing to its chemical stability (air and moisture-stable) and the presence of well-defined, pronounced hysteresis loops up to 8 K, as previously reported by Tong and co-workers.[46] Parameters such as saturation magnetisation (M_S), remanent magnetisation (M_R), and loop area (A) extracted from the hysteresis data have a strong possibility of showing temperature dependence, as faster magnetic relaxation at elevated temperatures progressively diminishes their values.[47] This strategy is conceptually straightforward and directly correlates with the slow relaxation dynamics that define SMM behaviour. However, it is not intended to replace luminescence thermometry, which remains simpler and more sensitive whenever strong optical signals and optical access are available, particularly above ~10 K. The value of the present approach lies in situations where optical readout is impractical, such as non-emissive or quenched complexes, or cryogenic device environments where optical access and direct thermometry are difficult. We have used SQUID here solely as a stable calibration platform; the concept can be transferred to miniaturised magnetic sensors (micro-Hall probes, nanoSQUIDs, magneto-optical or NV-based readouts) in future. The main limitations lie in the inherent collapse of hysteresis above the blocking temperature and the need for consistent sweep protocols. Thus, this method should be viewed as a complementary, cryogenic-range thermometric tool rather than a universal alternative to optical approaches (details in ESI, Section S6). Since hysteresis properties can be influenced by the magnetic field scan rate, we carried out a systematic scan rate-dependent study to assess the robustness of the method. The analysis shows that although the parameters exhibit minor scan-rate dependence, they follow the same trend and can be reliably employed for thermometry when the scan rate is kept constant. Throughout all scan rates, we observed remanent magnetisation and loop area providing superior sensitivity compared to saturation magnetisation. This proof-of-concept study highlights hysteresis-based thermometry as a promising novel strategy for cryogenic sensing in SMMs.

Results and discussion

Complex 1 was synthesised following the reported literature procedure[46] and characterised by single-crystal X-ray diffraction (SC-XRD), IR spectroscopy (Figure S1, ESI), powder XRD (Figure S2, ESI), and thermogravimetric analysis (TGA, Figure S3, ESI). The hysteresis data were recorded with a 200 Oe s^{-1} scan rate for complex 1. The magnetic hysteresis loops (Figure 1, S4, ESI) remain open at zero field up to 8 K. The corresponding thermometry parameters, such as saturation magnetisation (M_S), remanent magnetisation (M_R), and loop area (A), were extracted from the hysteresis data (details in SI).[47] The M_S and A showed a monotonic decrease with an increase in temperature (T) from 2 to 8 K (Figure 2 and S5, ESI). This reduction occurs because higher temperatures accelerate magnetic relaxation processes, allowing the spins to realign more rapidly with the applied magnetic field, resulting in a smaller saturation value and enclosed area.[48] However, in the case of M_R, a shallow maxima is observed around 2.5 K (M_R at 2.5 K exceeds that at 2.0 K, after which it decreases monotonically with temperature, Figure S5, ESI). This low-T dip might be attributed to efficient zero-field QTM at 2.0 K.[49] A slight increase in temperature reduces the exact resonance condition at H≈0, yielding higher M_R at 2.5 K. Above 2.5 K, M_R further decreases as thermally assisted relaxation starts to dominate at higher T (Figure S5a, ESI). For calibrating the temperature dependence of the thermometry parameters, we employed equation 1 (Table S1-S3, ESI).

$$\Delta = A_2 + \frac{A_1 - A_2}{1+\exp\left(\frac{T-T_o}{dT}\right)} \quad \text{.....Equation 1}$$

Where A_1 and A_2 are the values of thermometry parameters at low and high temperatures, respectively; T_o is the midpoint temperature where the transition occurs; and dT is the width of the transition (representing steepness). For saturation magnetisation (M_S), the full

View Article Online
DOI: 10.1039/D5TC03535J

ARTICLE

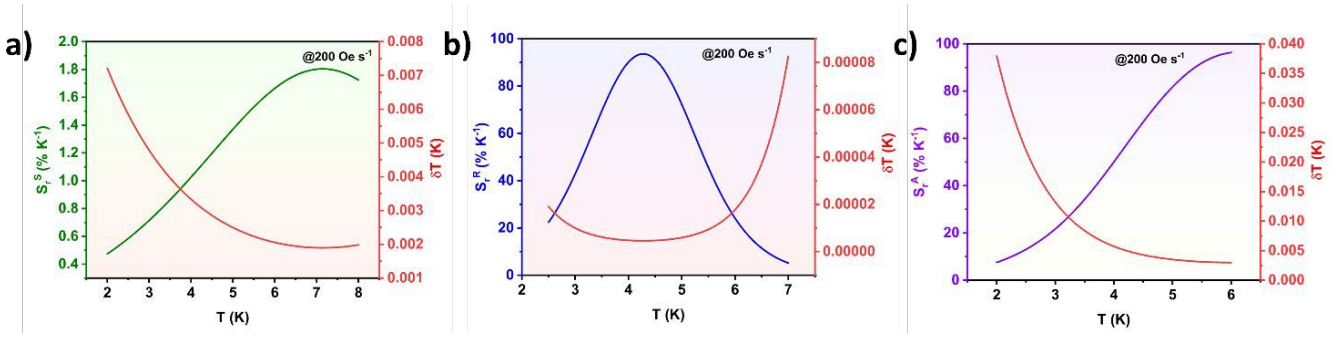

Figure 3: The temperature dependence of the relative thermal sensitivity and temperature uncertainty in complex 1 corresponding to a) saturation magnetisation, b) remanent magnetisation, and c) area.

2–8 K range was used for fitting. In contrast, for remanent magnetisation (M_R) and hysteresis loop area (A), the fitting was restricted to the ranges of 2.5–7 K and 2–6 K, respectively (Figure 2, S5, ESI). This restriction was necessary because, outside these temperature windows, the parameter values drop to below ~10% of their maximum, rendering the signal comparable to the experimental noise and thereby leading to unstable and non-reproducible fits. The relative thermal sensitivity (S_r) and temperature uncertainty (δT) were calculated using equations S1 and S2, ESI. The temperature-dependent hysteresis-based parameters reveal distinct thermometry behaviour. For saturation magnetisation, the relative sensitivity (S_r^S) initially increases with temperature, attaining a maximum of 1.8 % K^{-1} at 7.14 K, before gradually decreasing at higher temperatures (Figure 3a). Importantly, S_r^S remains above 1 % K^{-1} threshold throughout the 3.92 K to 8 K range, confirming its reliability in this temperature window. A comparable trend is observed for the remanent magnetisation-based sensitivity (S_r^R), which reaches a maximum of 93.6 % K^{-1} at 4.2 K (Figure 3b) with S_r^R > 1 % K^{-1} across the entire 2.5 K to 7 K range, underscoring its robustness as a thermometry parameter. In contrast, the loop area-derived sensitivity exhibits a monotonic increase from 2-6 K, peaking with 96.4 % K^{-1} at 6 K (Figure 3c). Throughout this interval, S_r^A continuously remains above 1 % K^{-1}, making the loop area a highly effective parameter for precise thermometry.

Overall, these results show that while saturation magnetisation provides moderate sensitivity across a broad temperature range, the loop area uniquely combines high sensitivity with wide applicability, making it the most versatile parameter for practical thermometry. Across all three approaches, the temperature uncertainty remained below 0.1 K, highlighting the accuracy of the hysteresis-based thermometry. From the overall analysis, a clear trend in thermal sensitivity is observed: loop area (S_r^A) > remanent magnetisation (S_r^R) > saturation magnetisation (S_r^S). This hierarchy can be understood by considering how much each parameter reflects the magnetisation changes. The loop area, as an integrated measure of the full hysteresis cycle, exhibits the highest sensitivity since thermal activation simultaneously modulates multiple magnetisation features. In contrast, remanent magnetisation reflects only the zero-field point, capturing a narrower thermal response. Saturation magnetisation is least sensitive, as strong fields align most spins, leaving thermal fluctuations with only a minor influence on the net magnetisation and thus the smallest relative temperature dependence. To check the applicability of our approach to other classes of SMMs, we synthesised $[Dy(L^{N6}_{phen})(Ph_3SiO)_2](PF_6)$ (Complex 2), as reported by Armenis *et al.*[50] The hysteresis-based thermometry for complex 2 yielded S_{max}^S of 1.1 % K^{-1} (at 4.3 K), and S_{max}^R of 31 % K^{-1} (at 3.6 K) (details in ESI, Figure S8-S9).

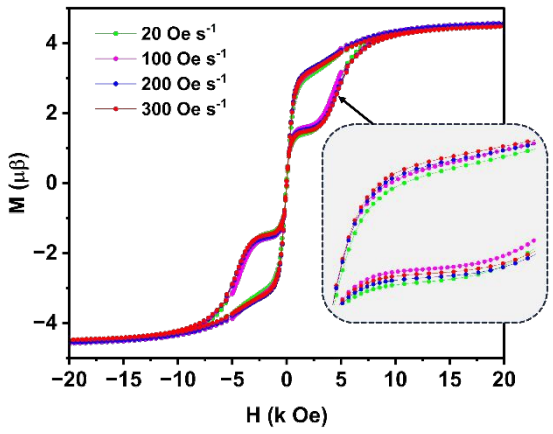

Figure 4: Variable scan rate hysteresis data of complex 1 at 2 K. Inset shows that a slower scan rate yields a smaller loop compared to the faster scan rate.

To further establish the broader applicability of hysteresis-based thermometry, we conducted scan-rate-dependent studies (20/100/200/300 Oe s^{-1}) on complex 1 (Figure 4, S4 ESI). Such an analysis is necessary because all these thermometry parameters are intrinsically governed by magnetic relaxation dynamics, and their quantitative values can vary depending on the applied scan rate. By systematically varying the scan rate, we can assess whether a) the

thermometry parameters exhibit consistent trends, b) the hierarchy ($S_r^A > S_r^R > S_r^S$) is preserved across all scan rates, and c) the approach remains valid under different measurement conditions. Together, these evaluations will provide a measure of the approach's overall robustness.

All three parameters exhibit comparable temperature-dependent trends for complex 1, with only modest changes in their absolute values (Figure 5, S6-S8, ESI). For saturation magnetisation (M_s), no difference is observed between 20, 100 and 200 Oe s^{-1}, indicating that Dy^{3+} moments fully align before significant relaxation occurs (Figure 5a). This points to a scan-rate threshold below which the process remains quasi-equilibrated. At higher rates (e.g., 300 Oe s^{-1}), the field

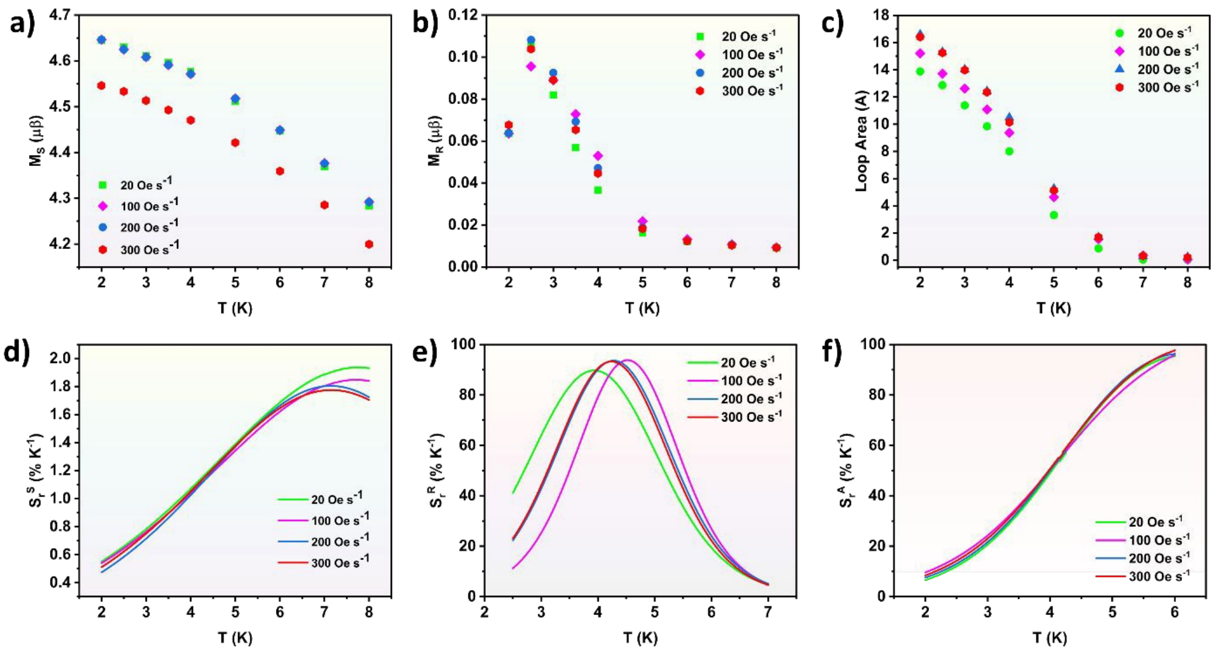

Figure 5: a), b), and c) Scan rate dependency of the thermometry parameters. d), e), and f) The temperature dependence of the relative thermal sensitivity under different scan rates (Scan rate: 20, 100, 200, and 300 Oe s^{-1}).

Table 1: List of single-molecule magnets showing thermometry below 10 K.

Formulae	S_{max} (T_{max})	~T range (S_r > 1 % K^{-1})	Thermometry Technique used	Ref
[Dy_2(bpm)(tfaa)$_6$]	1.8 (5.4)	5.4-85.5	Luminescence	30
{[Ho^{III}(4- pyridone)$_4$(H_2O)$_2$] [Co (CN)$_6$]}·nH_2O	6.9 (40)	2-140	Luminescence	51
{Tb^{III}[Co^{III}(CN)$_6$]}	5.28 (16)	6-92	Luminescence	42
[Ho(acac)$_3$(phen)]	95.3 (2.54)	1.55-5	Magnetic circular dichroism, MCD	44
[Dy(bbpen)Cl]	1.9 (7.7) from M_S 93.8 (4.5) from M_R 97.7 (6) from A	3.7-8 2.5-7 2-6	Hysteresis-based magneto-thermometry	This work

View Article Online
DOI: 10.1039/D5TC03535J

ARTICLE

change outpaces spin alignment, causing a slight reduction in M_s. Remanent magnetisation (M_r) shows only minor, non-systematic variations with scan rate across 20–300 Oe s^{-1}, with modest scatter at 2–4 K (Figure 5b). In contrast, the loop area is moderately scan-rate dependent (Figure 5c), where slower sweeps (20 and 100 Oe s^{-1}) allow greater relaxation and yield narrower loops, whereas faster sweeps (200 and 300 Oe s^{-1}) produce broader loops with larger area.[52] To assess the reliability of the approach, we compared S_r as a function of temperature at different scan rates (Table S4, Figure 5). All parameters show consistent profiles, confirming that the response is intrinsic to relaxation dynamics. Among them, the loop area is the most reproducible, with negligible scan-rate dependence, establishing it as the most reliable metric for cryogenic thermometry. The reported sensitivities for complex 1 are competitive with, and in some cases superior to, those reported for luminescence, MCD, and MCPL-based thermometry, highlighting the efficiency of hysteresis-loop features for cryogenic sensing (Table 1, S5, ESI).

Conclusions

This study presents a proof of concept showing that hysteresis-loop characteristics can act as intrinsic markers for thermometry in Dy-based SMMs. It reduces the need for modification of molecular design by incorporating other complicated properties, such as MCD or luminescence, in SMMs. By systematically analysing the relative sensitivities of saturation magnetisation, remanence magnetisation, and loop area, we obtained excellent magnetothermal sensitivities in a 2-8 K cryogenic range. Validating their applicability across scan-rate variations, we establish the loop area as the most reliable parameter for thermal readout. These findings provide new insight into the relaxation-governed thermal response of the system, while highlighting hysteresis-derived observables as a promising route for integrating molecular magnetism with precision low-temperature sensing. Looking forward, this approach could be relevant for device applications, such as calibration in dilution refrigerators or on-chip cryogenic temperature sensors.

Author contributions

SK and SS conceived the project idea. SS performed all the experiments and analysis and has written the manuscript with the help of SK.

Conflicts of interest

There are no conflicts to declare.

Data availability

The data supporting this article, including detailed materials, experimental procedures, characterisation methods, supplementary figures, tables, equations, and references, have been included as part of the ESI.†

Acknowledgements

S.K. thanks MoE, STARS Grant (Project No. MoE-STARS/STARS-2/2023-0301) for funding, IISER Bhopal for the instrumentation facility, and S.S. thanks PMRF for the research fellowship.

References

1. P.-Y. Liao, H.-R. Xing, Y.-L. Zhong, X.-N. Xu, P.-X. Lu, S.-D. Jiang, C.-H. Li, J.-L. Liu, R. A. Layfield and M.-L. Tong, *J. Am. Chem. Soc.*, 2025, **147**, 22714-22724.
2. C.-J. Yu, S. von Kugelgen, D. W. Laorenza and D. E. Freedman, *ACS Cent. Sci.*, 2021, **7**, 712-723.
3. X.-F. Ma, D. Zeng, C. Xu, S.-S. Bao and L.-M. Zheng, *Dalton Trans.*, 2023, **52**, 11913-11921.
4. Q.-C. Luo, Z.-H. Li, J. Lu and Y.-Z. Zheng, *Inorg. Chem. Front.*, 2025, **12**, 3695-3703.
5. B.-K. Ling, M. Chang, Y.-Q. Zhai, J. Deng, M. Kofu, H. Guo, J. Zhao, Z. Fu and Y.-Z. Zheng, *J. Am. Chem. Soc.*, 2025, **147**, 10935-10942.
6. F. Pointillart, K. Bernot, B. Le Guennic and O. Cador, *Chem. Commun.*, 2023, **59**, 8520-8531.
7. P. Kumar Sahu and S. Konar, *Chem. Eur. J.*, 2024, **30**, e202402439.
8. P. Kumar Sahu, A. Mondal and S. Konar, *Chem. Eur. J.*, 2023, **29**, e202203664.
9. P. Kumar Sahu, R. Kharel, S. Shome, S. Goswami and S. Konar, *Cord. Chem. Rev.*, 2023, **475**, 214871.
10. A. Gupta, S. Kapurwan, S. Prasad Bera, D. Jyoti Mondal, S. Shome and S. Konar, *Chem. Asian J.*, 2022, **17**, e202200622.
11. P. K. Sahu, S. Kapurwan and S. Konar, *Chem. Commun.*, 2025, **61**, 6105-6117.
12. A. S. Armenis, A. Mondal, S. R. Giblin, C. P. Raptopoulou, V. Psycharis, D. I. Alexandropoulos, J. Tang, R. A. Layfield and T. C. Stamatatos, *Chem. Commun.*, 2024, **60**, 12730-12733.
13. X.-D. Huang, X.-F. Ma, T. Shang, Y.-Q. Zhang and L.-M. Zheng, *Inorg. Chem.*, 2023, **62**, 1864-1874.
14. W.-J. Xu, Q.-C. Luo, Z.-H. Li, Y.-Q. Zhai and Y.-Z. Zheng, *Adv. Sci.*, 2024, **11**, 2308548.
15. N. El Beyrouti, F. Houard, M. Cordier, E. Trzop, S. Rigaut, B. Le Guennic, K. Bernot and L. Norel, *Chem. Commun.*, 2023, **59**, 5265-5268.
16. N. Jain, G. David, M. Cordier, Y. Suffren, B. L. Guennic, Y. Sarazin and K. Bernot, *ChemistryEurope*, **n/a**, 202500193.
17. D. A. Gálico and M. Murugesu, *Angew. Chem., Int. Ed.*, 2023, **62**, e202309152.

18. Q. Yang, J. Wu, C. Zhao, X. Ying, D.-M. Zhu, X. Guo, D. Liu, Y.-Q. Zhang and J. Tang, *Chem. Commun.*, 2025, **61**, 8751-8754.
19. C.-Y. Jin, Q. Zhang, J. Tang, P. Cheng and L. Li, *Dalton Trans.*, 2025, **54**, 7718-7725.
20. Y. Wang, Q.-C. Luo and Y.-Z. Zheng, *Angew. Chem., Int. Ed.*, 2024, **63**, e202407016.
21. J. J. Zakrzewski, M. Liberka, J. Wang, S. Chorazy and S.-i. Ohkoshi, *Chem. Rev.*, 2024, **124**, 5930-6050.
22. X.-D. Huang, X.-F. Ma and L.-M. Zheng, *Angew. Chem., Int. Ed.*, 2023, **62**, e202300088.
23. X.-F. Ma, Y. Guo, X.-D. Huang, G.-H. Wen, S.-S. Bao, Y.-Q. Zhang and L.-M. Zheng, *Dalton Trans.*, 2022, **51**, 12026-12030.
24. S. Shome, N. C. Maurya, M. Mukherjee, K. V. Adarsh and S. Konar, *Chem. Commun.*, 2025, **61**, 2337-2340.
25. H. Song, Z.-C. Wu, Y. Chen, N. Yang, Z. Zhang, M. D. Dramićanin and J. Li, *Adv. Opt. Mater.*, **n/a**, 2500107.
26. À. Tubau, L. Rodríguez, P. Pander, L. Weatherill, F. B. Dias, M. Font-Bardía and R. Vicente, *J. Mater. Chem. C*, 2024, **12**, 8127-8144.
27. V. Vieru, S. Gómez-Coca, E. Ruiz and L. F. Chibotaru, *Angew. Chem., Int. Ed.*, 2024, **63**, e202303146.
28. R. M. Diaz-Rodriguez, D. A. Gálico, D. Chartrand, E. A. Suturina and M. Murugesu, *J. Am. Chem. Soc.*, 2022, **144**, 912-921.
29. M. Tan, F. Li, N. Cao, H. Li, X. Wang, C. Zhang, D. Jaque and G. Chen, *Small*, 2020, **16**, 2004118.
30. D. Errulat, R. Marin, D. A. Gálico, K. L. M. Harriman, A. Pialat, B. Gabidullin, F. Iikawa, O. D. D. Couto, Jr., J. O. Moilanen, E. Hemmer, F. A. Sigoli and M. Murugesu, *ACS Cent. Sci.*, 2019, **5**, 1187-1198.
31. G. Brunet, R. Marin, M.-J. Monk, U. Resch-Genger, D. A. Gálico, F. A. Sigoli, E. A. Suturina, E. Hemmer and M. Murugesu, *Chem. Sci.*, 2019, **10**, 6799-6808.
32. R. Marin, D. A. Gálico, R. Gayfullina, J. O. Moilanen, L. D. Carlos, D. Jaque and M. Murugesu, *J. Mater. Chem. C*, 2022, **10**, 13946-13953.
33. A. A. Kitos, D. A. Gálico, R. Castañeda, J. S. Ovens, M. Murugesu and J. L. Brusso, *Inorg. Chem.*, 2020, **59**, 11061-11070.
34. A. A. Kitos, D. A. Gálico, N. Mavragani, R. Castañeda, J. O. Moilanen, J. L. Brusso and M. Murugesu, *Chem. Commun.*, 2021, **57**, 7818-7821.
35. R. A. S. Ferreira, E. Mamontova, A. M. P. Botas, M. Shestakov, J. Vanacken, V. Moshchalkov, Y. Guari, L. F. Chibotaru, D. Luneau, P. S. André, J. Larionova, J. Long and L. D. Carlos, *Adv. Opt. Mater.*, 2021, **9**, 2101495.
36. K. Karachousos-Spiliotakopoulos, V. Tangoulis, N. Panagiotou, A. Tasiopoulos, E. Moreno-Pineda, W. Wernsdorfer, M. Schulze, A. M. P. Botas and L. D. Carlos, *Dalton Trans.*, 2022, **51**, 8208-8216.
37. K. Karachousos-Spiliotakopoulos, V. Tangoulis, N. Panagiotou, A. Tasiopoulos, V. Nastopoulos, E. Moreno-Pineda, W. Wernsdorfer, M. Schulze, A. M. P. Botas and L. D. Carlos, *Inorg. Chem.*, 2022, **61**, 18629-18639.
38. K. Kumar, O. Stefanczyk, K. Nakabayashi, K. Imoto, Y. Oki and S.-i. Ohkoshi, *Adv. Opt. Mater.*, 2022, **10**, 2101721.
39. K. Kumar, D. Abe, K. Komori-Orisaku, O. Stefańczyk, K. Nakabayashi, J. R. Shakirova, S. P. Tunik and S.-i. Ohkoshi, *RSC Adv.*, 2019, **9**, 23444-23449.
40. J. Wang, J. J. Zakrzewski, M. Heczko, M. Zychowicz, K. Nakagawa, K. Nakabayashi, B. Sieklucka, S. Chorazy and S.-i. Ohkoshi, *J. Am. Chem. Soc.*, 2020, **142**, 3970-3979.
41. K. Kumar, O. Stefanczyk, S. Chorazy, K. Nakabayashi and S.-i. Ohkoshi, *Adv. Opt. Mater.*, 2022, **10**, 2201675.
42. J. Wang, J. J. Zakrzewski, M. Zychowicz, Y. Xin, H. Tokoro, S. Chorazy and S.-i. Ohkoshi, *Angew. Chem., Int. Ed.*, 2023, **62**, e202306372.
43. S. Zanella, M. Aragon-Alberti, C. D. S. Brite, F. Salles, L. D. Carlos and J. Long, *Angew. Chem., Int. Ed.*, 2023, **62**, e202306970.
44. D. A. Gálico and M. Murugesu, *Angew. Chem., Int. Ed.*, 2025, **64**, e202505806.
45. A. G. Bispo-Jr, *Cord. Chem. Rev.*, 2025, **537**, 216685.
46. J. Liu, Y.-C. Chen, J.-L. Liu, V. Vieru, L. Ungur, J.-H. Jia, L. F. Chibotaru, Y. Lan, W. Wernsdorfer, S. Gao, X.-M. Chen and M.-L. Tong, *J. Am. Chem. Soc.*, 2016, **138**, 5441-5450.
47. Y. Yu and L. Tauxe, *Geochemistry, Geophysics, Geosystems*, 2005, **6**.
48. Y. Yu, L. Tauxe and B. M. Moskowitz, *Geochemistry, Geophysics, Geosystems*, 2004, **5**.
49. D. N. Woodruff, R. E. P. Winpenny and R. A. Layfield, *Chem. Rev.*, 2013, **113**, 5110-5148.
50. A. S. Armenis, A. Mondal, S. R. Giblin, D. I. Alexandropoulos, J. Tang, R. A. Layfield and T. C. Stamatatos, *Inorg. Chem. Front.*, 2025, **12**, 1214-1224.
51. J. Wang, J. J. Zakrzewski, M. Zychowicz, V. Vieru, L. F. Chibotaru, K. Nakabayashi, S. Chorazy and S.-i. Ohkoshi, *Chem. Sci.*, 2021, **12**, 730-741.
52. M. S. Raju, K. Paillot, I. Breslavetz, G. Novitchi, G. L. J. A. Rikken, C. Train and M. Atzori, *J. Am. Chem. Soc.*, 2024, **146**, 23616-23624.

View Article Online
DOI: 10.1039/D5TC03535J

Data Availability Statement

The data supporting this article have been included as part of the Supplementary Information.